UNIVERSITÀ POLITECNICA DELLE MARCHE
Repository ISTITUZIONALE

Designing new ferrite/manganite nanocomposites

This is the peer reviewd version of the followng article:

Original
Designing new ferrite/manganite nanocomposites / Muscas, G.; Anil Kumar, P.; Barucca, Gianni; Concas, G.; Varvaro, G.; Mathieu, R; Peddis, D.. - In: NANOSCALE. - ISSN 2040-3364. - ELETTRONICO. - 8:4(2016), pp. 2081-2089. [10.1039/c5nr07572f]

Availability:
This version is available at: 11566/233897 since: 2022-05-23T16:10:07Z

Publisher:

Published
DOI:10.1039/c5nr07572f

Terms of use:

The terms and conditions for the reuse of this version of the manuscript are specified in the publishing policy. The use of copyrighted works requires the consent of the rights' holder (author or publisher). Works made available under a Creative Commons license or a Publisher's custom-made license can be used according to the terms and conditions contained therein. See editor's website for further information and terms and conditions.
This item was downloaded from IRIS Università Politecnica delle Marche (https://iris.univpm.it). When citing, please refer to the published version.

(Article begins on next page)

28 February 2025

Designing new ferrite/manganite nanocomposites with tunable magnetic and electrical properties

G. Muscas[a,b,c], P. Anil Kumar[a], G. Barucca[d], G. Concas[c], G. Varvaro[b], R. Mathieu*[a] and D. Peddis*[b]

[a]Department of Engineering Sciences, Uppsala University, Box 534, SE-751 21, Uppsala, Sweden

[b]Istituto di Struttura della Materia - CNR, 00015 Monterotondo Scalo (RM), Italy

[c]Dipartimento di Fisica, Università di Cagliari, S.P. Monserrato-Sestu km 0.700, 09042, Monserrato, Italy

[d]Dipartimento di Scienze e Ingegneria della Materia, dell'Ambiente ed Urbanistica, Università Politecnica delle Marche, via Brecce Bianche 12, Ancona, Italy

1 Abstract

Two kinds of nanocomposites of transition metal oxides were synthesized and investigated. Each nanocomposite comprises nanoparticles of $La_{0.67}Ca_{0.33}MnO_3$ and $CoFe_2O_4$ in similar volume fractions, however arranged with different morphology. The temperature-dependent magnetic and electrical properties of the two systems are found to greatly differ, suggesting different degrees of interaction and coupling of their constituents. This is confirmed by magnetic field-dependent experiments, which reveal contrasted magnetization reversal and magnetoresistance in the systems. We discuss this morphology-physical properties relationship, and the possibility to further tune the magnetism and magnetotransport in such nanocomposites.

2 Introduction

Transition metal oxides represent an interesting class of materials due to their cross correlated electronic and magnetic properties [1,2]. For example magnetic oxides have been shown to display many interesting (magneto)transport properties, such as the colossal magnetoresistance (CMR) [3], tunnel magnetoresistance (TMR) [4], electroresistance [5], as well as magnetodielectric [6] and magnetoelectric [7] effects.

In the last years it was reported that composites including two or more transition metal oxides may be very attractive as their magnetic and electrical properties could be tuned or controlled owing to the interaction of its constituents. For example multiferroic and/or magnetoelectric properties were demonstrated in nanostructures consisting of $CoFe_2O_4$ pillars embedded in $BaTiO_3$ matrix [8] or $BiFeO_3$ pillars embedded in $CoFe_2O_4$ [9]. It was also found that the magneto-transport, and more particularly the TMR, can be tuned in composites formed of micrometer-scale mixtures of strongly correlated materials such as (La,Sr)MnO_3 and $CoFe_2O_4$ [10], owing to the dipolar field exerted by the $CoFe_2O_4$ particles onto the (La,Sr)MnO_3 ones. In a different system comprising $Fe_3O_4/CoFe_2O_4$ core/shell nanoparticles the TMR is dominated by the interface exchange coupling [4].

In the present paper, we show that the electrical and magnetic response of composites of strongly correlated oxides may be tuned by controlling the materials combination at nanoscale. To prepare nanocomposites two synthetic strategies has been used: mechanical mixing of two different nanoparticle systems (N-MIX) and growing nanoparticles of one of the system around nanoparticles of the other (NC) in order to maximize the contact between nanomaterials. NC sample was synthesized by a simple and low cost synthetic approach, based on seed mediated growth self-combustion method, allowing to produce high quantity of samples with well controlled morphology

We present the complete structural and morphological characterization of N-MIX and NC as well as their magnetic and magnetotransport properties to illustrate the relationship between morpho-structural features and physical properties. We have chosen to combine nanoparticles of the well-known $La_{0.67}Ca_{0.33}MnO_3$ (LCMO) and $CoFe_2O_4$ (CFO) oxides, using the LCMO-CFO as a model system to illustrate our synthesis approach.

3 Experimental

3.1 Synthesis

3.1.1 N-MIX sample

$La_{0.67}Ca_{0.33}MnO_3$ nanoparticles (N-LCMO) were prepared by a polyol sol-gel approach [11], while $CoFe_2O_4$ nanoparticles (N-CFO) were prepared by polyol process [12–14] (see Supplementary information for more details). To prepare the N-MIX sample 80 mg of N-LCMO and 20 mg of N-CFO (effective weight

considering also organic coating) were grounded in a mortar with acetone to obtain a fine mixture of the two powders.

3.1.2 NC sample

In order to improve the magnetic coupling between $La_{0.67}Ca_{0.33}MnO_3$ (LCMO) and $CoFe_2O_4$ (CFO) phases, a nanocomposite (NC) was prepared by a seed mediated growth self-combustion method. N-CFO nanoparticles (20% in weight of the final product) were dispersed in ethylene glycol (EG) (10 ml) to be used as seeds for the growth of LCMO nanoparticles. 4.6 mmol of lanthanum (III) nitrate hexahydrate (Fluka analytical, > 99 %), 2.3 mmol of calcium (II) nitrate tetrahydrate (Sigma Aldrich, 99 %) and 6.9 mmol of Manganese (II) nitrate tetrahydrate (Sigma Aldrich, > 97 %) were added to the EG solution (Sigma Aldrich, 99.8 %) with an amount of distilled water equal to their weight. The homogenous dispersion of the CFO seeds and the complete solubilization of the reactants were obtained keeping the solution on a hotplate at 80 °C, under magnetic stirring. Then, the temperature of the solution was raised and kept at 150°C, until a thick and dense gel was formed, tuning the stirring speed in order to obtain a homogenous CFO dispersion. Finally, the temperature was increased to 300 °C and after few minutes, the gel combustion occured, producing a very soft and porous grey powder. To ensure the complete crystallization of LCMO, the product was calcinated in an oven at 550 °C for 2 hours.

To perform resistivity measurements, both N-MIX and NC were pressed (30 kN) in form of pellet, then they were calcinated at 550 °C for 2 h, in order to obtain a better connectivity among particles and so an improved conductivity through the LCMO phase. All the structural, morphological and magnetic characterizations have been performed on powder coming from pellet.

3.2 Experimental techniques and data treatments

X-ray diffraction (XRD) patterns were collected with a Bruker Davinci instrument operating with a Cu K_α radiation source. The samples were prepared by depositing an ethanol dispersion of nanoparticles on a zero background holder. The cell parameters and the average size of the coherent crystalline domain were determined by XRD Rietveld refinement using MAUD [15,16]. To determine the instrumental broadening contribution, a polycrystalline and strain-free sample of Al_2O_3 has been used as standard.

Transmission electron microscopy (TEM) analyses were performed by a Philips CM200 microscope operating at 200 kV and equipped with a LaB_6 filament. For TEM observations, the samples, in form of powder, were prepared using the following procedure. A small quantity of powder was dispersed in isopropyl alcohol and subjected to ultrasonic agitation for about one minute. A drop of the suspension was deposited on a commercial TEM grid covered with a thin carbon film; finally the grid was kept in air until complete isopropyl alcohol evaporation.

Energy dispersive spectrometry (EDS) measurements were carried out in a field emission Zeiss Supra 40 scanning electron microscope equipped with a Bruker Quantax 200 microanalysis. Before analysis, the

samples were attached to an aluminum stub by a self-adhesive carbon disc and covered with a thin carbon film in order to increase the electrical conductivity.

DC magnetization measurements were carried out by a Quantum Design superconducting quantum interference device (SQUID) magnetometer, equipped with a superconducting magnet (H_{max} ±5 T). To avoid any displacement of the nanoparticles during the measurements, the samples, in form of powders, were immobilized in an epoxy resin. For the magnetization vs. temperature measurements, the Zero Field Cooled (ZFC), Field Cooled (FC), and Thermo-Remanent Magnetization (TRM) protocols were used. To perform ZFC measurements, the sample was first cooled from room temperature to 5 K in zero field; then the magnetization (M_{ZFC}) was recorded warming up from 5 to 300 K, with a static applied magnetic field, while the M_{FC} was recorded during the subsequent cooling from 300 to 5 K. In the TRM measurements, the sample was cooled from room temperature to 5 K in an external magnetic field, then the field was turned off and the magnetization was measured warming up from 5 to 300 K.

Resistivity measurements were performed with Quantum design physical property measurement system (PPMS) equipped with the resistivity option. The sample, in form of pellet, was fixed with varnish on a sapphire substrate. The measurements were conducted in a four-probe geometry with constant current passing through the sample.

4 Results and Discussion

4.1 Structure and Morphology

XRD patterns of N-LCMO and N-CFO samples (**figure S1**) show reflections of $La_{0.67}Ca_{0.33}MnO_3$ perovskite (PDF card 01-089-6933) and $CoFe_2O_4$ cubic spinel oxide (PDF card 01-079-1744) structures, respectively. No reflections of any other phase are detected.

According to TEM analysis, N-LCMO sample is composed of roughly spherical nanoparticles, having size ranging between 10 and 50 nm (**figure S2a**). The particles are strongly aggregated and the aggregates have a high porosity (**figure S2b**). The presence of pores is an expected result of the combustion of the organic material and of the gas formation during the self-combustion process. The introduction of the self-combustion step on the hotplate at 300°C, before proceeding with calcination, allows to conduce it at a relatively low temperature (550°C) (**figure S3**) and with a shorter time (2h) with respect to what is usually employed[17–19]. This relative low temperature has been demonstrated to be enough to obtain high crystalline single-phase perovskite manganite with particles size among the smallest (± 28 nm) reported in literature[18,19]. It is worth mentioning that the LCMO composition has been confirmed by EDS analysis, within the experimental error (±5%). N-CFO particles exhibit an average diameter of ~ 5 nm, with a narrow size distribution and a high degree of crystallinity (**figure S2c and S2d**). Despite the polyol coating, a strong aggregation among particles is observed.

XRD patterns of both N-MIX and NC samples (**figure S1**) show only the main reflections of $La_{0.67}Ca_{0.33}MnO_3$ and $CoFe_2O_4$ crystalline structures and no other phases are detected. The weight fraction of CFO and LCMO, estimated by the Rietveld analysis (**table 1**) suggests a ratio of ≈ 30% / 70% and 40% / 60% for N-MIX and NC respectively. In both samples, EDS analysis shows that the stoichiometric formula of the original LCMO and CFO phases have been maintained.

TEM bright field images of the N-MIX sample are shown in **figure 1a-c**. The sample consists of two kinds of particle aggregates randomly distributed. In particular, in **figure 1c** the blue and red circles indicate aggregates of LCMO and CFO particles, respectively; the CFO aggregates show average size around 300 nm, while LCMO ones are generally slightly larger. In figure 1d is imaged a typical selected area electron diffraction (SAED) pattern of a CFO aggregate. It consists of continuous diffraction rings indicating that CFO nanoparticles are crystalline and randomly oriented. Measuring the radius of the rings and calculating the associated interplanar distances, the crystallographic phase of the CFO nanoparticles can be identified in the cubic $CoFe_2O_4$ spinel oxide. It is important to stress that an intimate mixing between the two phases has never been observed in N-MIX sample. On the other hand, the NC sample shows clearly a different morphology: LCMO particles are generally less aggregated, and there is no trace of CFO particles at a first sight (**figure 1e and f**). The presence of the CFO phase is revealed in **figure 1g**, which shows a ~~selected~~ SAED pattern corresponding to the sample area imaged in **figure 1f**. It consists of intense diffraction spots, randomly distributed, and weak diffraction rings. Analyzing the interplanar distances obtained from SAED, it is possible to associate the origin of the intense diffraction spots to the presence of quite large LCMO crystals and the diffraction rings to the presence of small CFO crystals randomly oriented. Finally, **figure 1h** is the corresponding dark field image of **figure 1f**, obtained using part of the first diffraction ring of **figure 1g**; in this way the CFO particles responsible for that part of the diffraction ring, appear bright in the image. This shows that the CFO particles do not form aggregates and they are homogeneously distributed in the LCMO phase. It is important to stress that many dark field images have been taken in different areas of the sample, using different parts of the visible diffraction rings and the same CFO particles distribution has always been observed. The size of the cobalt ferrite particles is in perfect agreement with that measured for the N-CFO sample; instead, LCMO particles appear, in some cases, larger than those in the N-LCMO one. Concerning the particles size, TEM analyses confirm XRD results. In particular in table 1 are reported the particles sizes obtained by XRD measurements. It is worth to note that sample N-MIX presents larger mean crystallite size for both LCMO and CFO phases compared to the original untreated compounds (**table 1**). On the other hand, sample NC shows LCMO particles only slightly larger than the untreated ones while the CFO particles keep their original size within the experimental error. This suggests that in NC sample the good dispersion of CFO particles inside the LCMO matrix protects them, avoiding their growth during the pellet calcination step.

4.2 Reversal mechanism of the magnetization

The ZFC-FC curves were measured in the interval 5-300 K with an applied field of 2.5 mT. For N-MIX sample (**figure 2c**), on cooling down, the magnetization sharply decreases in both curves around ≈ 260 K (**figure2a**), evidence of the ferromagnetic to paramagnetic (FM / PM) transition. This temperature corresponds to the T_C usually reported for bulk LCMO of this La/Ca composition [20,21], furthermore, also N-LCMO sample shows the same behavior (**figure S6a** and **b**). No evidence of superparamagnetic (SPM) transition related to CFO nanoparticles is identified, despite CFO presence has been clearly demonstrated by XRD and TEM. Considering the peak produced by the blocking temperature of pure CFO (**figure 2b**), it is reasonable to think that its contribution in ZFC-FC curves, should produce a signal that is hidden by those much stronger of LCMO, which represents ≈ 80% of the sample. To enforce this hypothesis, an artificial curve has been created by summing the contribution of CFO and LCMO curves with a weight ratio of 20 and 80 %, respectively (**figure S5**). As expected, this curve exhibited the same trend of N-MIX.

Sample NC presents a ZFC curve with two clear peaks (**figure 2d**). The peak at ≈ 240 K reproduces exactly that of CFO phase (**figure 2b**). On the other hand, the peak around ≈ 110 K could be related to the presence of the nanostructured LCMO phase. This hypothesis is confirmed comparing the ZFC curve with that of a further composite, labelled as NC2, prepared with the same procedure of NC, but employing only 5% in weight of CFO phase. Its ZFC curve exhibits the dominant contribution of nanosized LCMO particles (**figure 2d**); the FM/PM transition is shifted toward lower temperature, with a drop in magnetization value, which induces a peak exactly around ≈ 110 K. Such behavior is confirmed and better described by TRM measurements [22], as discussed in Supplementary information.

The field dependence of magnetization recorded at 5 K shows a clearly different behavior for N-MIX and NC samples (**figure 3a**). The loop shape of the N-MIX sample is ~~at~~ close to a simple superposition of the hysteresis loops of pure CFO and LCMO phases (**figure 3b** and **c**) suggesting a lack of coupling between the two phases. Indeed the coercive field $\mu_0 H_C$ reproduces the same value of N-LCMO, while the saturation field $\mu_0 H_{sat}$, which can be considered as the maximum field that is necessary to apply to reverse even the moment of the particles with the highest anisotropy energy, is quite close to that of the pure CFO component (**figure 3c** and **table 2**). $\mu_0 H_{sat}$ has been measured as the point in which the difference between the branches is under the 1% of their maximum value[23]. Both LCMO and CFO components are clearly detectable, but they appear acting individually, without a significant coupling. On the other hand, the M(H) curve for the NC sample (**figure 3a**) exhibits a nearly single phase behavior, indicating a strong coupling between LCMO and CFO phases. A closer inspection indicates the hysteresis loop is slightly constricted. This suggests a magnetic behavior that is placed in the transition region between that of a rigid magnet, where the soft and hard phases reverse coherently, and that of an exchange-spring system, where the soft phase reverses first and support the switching of the hard component [24].

It should be underlined that the saturation magnetization values (**table 2**) of both samples are lower with respect the bulk LCMO (≈ 97 A m^2 kg^{-1}), in agreement with previous literature [25–27] supposing a magnetically disordered surface as the origin of saturation magnetization reduction in nanoparticles.

A more detailed investigation of the magnetization reversal has been performed analyzing the field dependence of the remanent magnetization measured at 5 K by IRM and DCD protocols (**table 2** and **figure S7, in supporting information**, for pure phases). The differentiated remanence curve of M_{DCD} with respect to $\mu_0 H_{reverse}$, represents the irreversible component of the susceptibility ($\chi_{irr} = dM_{DCD}/d\mu_0 H$). This quantity can be considered as a measure of the energy barrier distribution which, in a nanoparticles system, is associated with a distribution of particles switching field (SFD), defined as the field necessary to overcome the energy barrier during an irreversible reversal process. It is worth mentioning that the switching field would be equivalent to the coercivity in the absence of reversible processes [28–30]. The SFD of sample N-MIX (**figure 3d**) presents a strong contribution centered at low field (≈ 0.05 T) as for the pure LCMO, and only a very weak signal at high field (≈ 1.73 T) related to CFO phase. This value is even larger than the average switching field of the pure phase, the reason of which can be ascribed to the thermal treatment at 550 °C. As previously demonstrated such thermal treatment can induce a modification in inversion degree (i.e., Co^{2+} and Fe^{3+} site occupancy) , leading to an increase of magnetic anisotropy [30]. It is a matter of fact that sample N-MIX shows the individual contribution of these two phases without a clear coupling. On the other hand, sample NC presents a different picture (**figure 3d**): the contributions of the pure phases are visible but the two average switching fields are shifted closer with respect the original pure phases, as results of a strong coupling between them.

The IRM and DCD magnetization curves are compared in so called *ΔM-plots* [31] in order to study the nature of interparticle magnetic interactions (**table 2**, see **supporting information** for detailed description). Both N-MIX and NC show plots with dips (**figure S8c and d**), thus revealing the prevalence of dipolar interactions [32–34], while local exchange interactions cannot be excluded. Furthermore, sample N-MIX exhibits two different dips in the *ΔM* plots, indicating two mechanisms of interaction, which are compatible with the independent interactions of LCMO and CFO particles. This is in agreement with the morphology evidenced in the TEM images, where LCMO and CFO particles form distinct single-phase aggregates where particles mainly interact among themselves. In a stark contrast, sample NC shows a single broad signal centered at ≈ 1.25 T, thus confirming an almost single-phase interaction mechanism between LCMO and CFO, which is strongly related to the morphological structure of this sample. The coupling between CFO and LCMO particles is strong enough to shift the reversal process of the LCMO towards higher fields, far above its original coercive field. It allows an almost single magnetization switching, mostly related to the high field process of the CFO component, remarking the same behavior shown in M(H) curve.

4.3 Magnetotransport

Coherently with the differences in morpho-structural and magnetic properties, the two nanocomposites exhibit a well distinct electrical transport behavior. R Vs T curve of sample N-MIX (**figure 4a**) shows a peak at a temperature T_R (≈ 123 K) lower than the T_C (≈ 260 K) of LCMO component, when the metal-insulator transition occurs. This behavior is typical for systems in which the resistivity is dominated by grain boundaries [35] and/or surface effects[36]. The measured magneto-resistance (MR) effect (**figure 4b**) shows a continuous increment down to ≈ 120 K, when all material undergoes the FM-metallic transition. Then it remains almost constant down to ≈ 50 K; on further lowering of temperature an upturn is observed in resistance probably reflecting the Coulomb blockade phenomenon that is seen in metallic nanoparticles [37]. The thermal energy of the charge carriers at a such low temperatures cannot overcome the coulomb repulsion and hence reduces the probability of tunneling [38], leading to a new insulating regime. Finally, the application of an external field induces a common spin orientation reducing the spin scattering [3], as result the overall resistivity is reduced (**figure 4a**).

On the other hand, NC sample shows high resistance values with a strong increment on reducing the temperature (**figure 4a**), reaching an unmeasurably high value below 180 K. Such strong resistivity can be related to the specific structure of the sample. The CFO component in sample N-MIX does not increase the overall resistivity, since the CFO agglomerates do not represent a significant obstacle for the electric flow within the LCMO phase. On the other hand, the core/shell-like structure of NC owns a very fine and homogenous distribution of the insulating CFO, which promotes an insulating character for the composite [54]. Furthermore, only a weak magneto-resistance is visible and the two curves with and without applied field are almost perfectly superimposed. One should note that cooling down the sample, the MR curve exhibits a small negative peak (-8 %) at ≈ 240 K, which could be related to the onset of the FM ordering. Analyzing the R Vs T curve of NC2 sample, an intermediate behavior is observed (**figure 4a** and **b**). A magnetoresistance effect is clearly visible but still the absolute value of resistance can be measured only down to ≈ 130 K. This suggests that the conducting behavior of such core/shell composites can be tuned, e.g., modifying the CFO/LCMO ratio and/or particles size.

The MR behavior of N-MIX sample was further investigated by collecting R Vs. H loops at constant temperatures. As shown in **figure 4c** the sample at 5 K shows a conventional behavior; sweeping the field from 8 to -8 T, a peak in MR is visible with a negative applied field $\mu_0 H_C^{MR}$ and sweeping in the opposite direction the peaks appears with a positive $\mu_0 H_C^{MR}$. This is in contradiction to the inversion of R-H loops observed in macroscopic composite of LSMO and CFO [10] . However, measuring the R-H loops at higher temperatures leads to a decrease in $\mu_0 H_C^{MR}$ and interestingly the R-H loop is inversed for temperature above 100 K. The MR peak occurs before the switching of the direction of the applied field, reaching a maximum opposite value around 150 K (**figure 4d**). Such dipolar biasing effect [10] occurs at a low applied field, when the residual magnetization of CFO produces a stronger local dipolar field that leads to the

antiparallel coupling of LCMO, which switches its magnetization, before the inversion of the external field H_{ext}, but the dipolar field effect disappears under 100 K.

5 Conclusions

We report the novel design of nanocomposites of transition metal oxides with tailored magnetic and electrical properties. We illustrate the synthesis methods and the relationship between morphological and physical properties using the well-known $La_{0.67}Ca_{0.33}MnO_3$ (LCMO) and $CoFe_2O_4$ (CFO) oxides as model systems. The properties of a mechanical mixture of LCMO and CFO phases are compared with those of a nanocomposite prepared by a new synthetic approach. Structural and morphological characterization clearly shows a strong aggregation of CFO nanoparticles in N-MIX sample, hindering an intimate contact between the two magnetic phases. On the other hand, NC sample shows a very homogeneous morphology, with CFO nanoparticles well dispersed in the LCMO matrix. Consequently, a strong magnetic coupling has been shown by the NC sample, with magnetic behavior that can be considered in the transition region between that of a rigid magnet and that of an exchange-spring system. On the other hand, a very poor coupling has been evidenced for the N-MIX, with independent reversal mechanism for LCMO and CFO phases. Similarly, both samples show clearly different electrical behavior. While the NC composite is highly insulating, magnetoresistance and dipolar biasing effects are observed in the N-MIX sample.

$La_{0.67}Ca_{0.33}MnO_3$-$CoFe_2O_4$ samples have been used as a model system to illustrate this novel approach, and they represent a first attempt to produce such new nanocomposites of strongly correlated materials. Further improvement can be achieved by tuning the relative amount of CFO and its particles size. As well as creating an inverse core-shell structure, where LCMO represents the core surrounded by a thin CFO layer.

Acknowledgments

G. Muscas gratefully acknowledges Sardinia Regional Government for the financial support of his PhD scholarship (P.O.R. Sardegna F.S.E. Operational Program of the Autonomous Region of Sardinia, European Social Fund 2007-2013 **- Axis IV Human Resources, Objective l.3, Line of Activity l.3.1.)**

G. Muscas gratefully acknowledges the C.M. Lerici foundation for the financial support for its research activity at the Uppsala University.

P. Anil Kumar and R. Mathieu acknowledge the Swedish Research Council (VR), and the Göran Gustafsson foundation.

References

1 Y. Tokura and N. Nagaosa, *Science (80-.).*, 2000, **288**, 462–468.

2 E. Dagotto, *Science*, 2005, **309**, 257–62.

3 Y. Tokura and Y. Tomioka, *J. Magn. Magn. Mater.*, 1999, **200**, 1–23.

4 P. Anil Kumar, S. Ray, S. Chakraverty and D. D. Sarma, *Appl. Phys. Lett.*, 2013, **103**, 102406.

5 T. Fujii, M. Kawasaki, A. Sawa, H. Akoh, Y. Kawazoe and Y. Tokura, *Appl. Phys. Lett.*, 2005, **86**, 012107.

6 D. Choudhury, P. Mandal, R. Mathieu, A. Hazarika, S. Rajan, A. Sundaresan, U. V. Waghmare, R. Knut, O. Karis, P. Nordblad and D. D. Sarma, *Phys. Rev. Lett.*, 2012, **108**, 127201.

7 D. Khomskii, *Physics (College. Park. Md).*, 2009, **2**.

8 H. Zheng, J. Wang, S. E. Lofland, Z. Ma, L. Mohaddes-Ardabili, T. Zhao, L. Salamanca-Riba, S. R. Shinde, S. B. Ogale, F. Bai, D. Viehland, Y. Jia, D. G. Schlom, M. Wuttig, a Roytburd and R. Ramesh, *Science*, 2004, **303**, 661–3.

9 R. K. Zheng, H. Gu, B. Xu and X. X. Zhang, *J. Phys. Condens. Matter*, 2006, **18**, 5905–10.

10 P. Anil Kumar and D. D. Sarma, *Appl. Phys. Lett.*, 2012, **100**, 262407.

11 T. Sarkar, a K. Raychaudhuri, a K. Bera and S. M. Yusuf, *New J. Phys.*, 2010, **12**, 123026.

12 F. Fiévet and R. Brayner, in *Nanomaterials: A Danger or a Promise?*, eds. R. Brayner, F. Fiévet and T. Coradin, Springer London, 2013, pp. 1–25.

13 S. Ammar, A. Helfen and N. Jouini, *J. Mater. Chem.*, 2001, 186–192.

14 S. Chkoundali, S. Ammar, N. Jouini, F. Fiévet, P. Molinié, M. Danot, F. Villain and J.-M. Grenèche, *J. Phys. Condens. Matter*, 2004, **16**, 4357–4372.

15 L. Luterotti, .

16 L. Lutterotti, S. Matthies and H. R. Wenk, *IUCr Newsl. CPD*, 1999, **21**.

17 T. Sarkar, B. Ghosh, A. K. Raychaudhuri and T. Chatterji, *Phys. Rev. B*, 2008, **77**, 235112.

18 K. Shankar and A. Raychaudhuri, *J. Mater. Res.*, 2006, **21**, 27–33.

19 S. Xi, W. Lu and Y. Sun, *J. Appl. Phys.*, 2012, **111**, 063922.

20 Y. Tokura, Ed., *Colossal magnetoresistive oxides*, CRC Press, 2000.

21 L. Liu, J. J. Zheng, S. L. Yuan, Z. M. Tian and C. H. Wang, *J. Nanoparticle Res.*, 2010, **13**, 2305–2310.

22 G. Muscas, G. Concas, C. Cannas, A. Musinu, A. Ardu, F. Orrù, D. Fiorani, S. Laureti, D. Rinaldi, G. Piccaluga and D. Peddis, *J. Phys. Chem. C*, 2013, **117**, 23378–23384.

23 R. Kodama, A. Berkowitz, E. M. Jr, S. Foner and E. McNiff, *Phys. Rev. Lett.*, 1996, **77**, 394–397.

24 A. López-Ortega, M. Estrader, G. Salazar-Alvarez, A. G. Roca and J. Nogués, *Phys. Rep.*, 2015, **553**, 1–32.

25 A. Martinelli, M. Ferretti, C. Castellano, M. R. Cimberle, R. Masini, D. Peddis and C. Ritter, *J. Phys. Condens. Matter*, 2013, **25**, 176003.

26 D. Markovic, V. Kusigerski, M. Tadic, J. Blanusa, M. V. Antisari and V. Spasojevic, *Scr. Mater.*, 2008, **59**, 35–38.

27 M. A. Lopez-Quintela, L. E. Hueso, J. Rivas and F. Rivadulla, *Nanotechnology*, 2003, **14**, 212–219.

28 K. O'Grady and R. W. Chantrelll, *Int. Work. Stud. Magn. Prop. Fine Part. their Relev. to Mater. Sci.*, 1991, 93–102.

29 C. Binns, Ed., *Nanomagnetism: Fundamentals and Applications*, Elsevier, Oxford, 2014.

30 D. Peddis, F. Orrù, A. Ardu, C. Cannas, A. Musinu and G. Piccaluga, *Chem. Mater.*, 2012, **24**, 1062–1071.

31 E. P. Wohlfarth, *J. Appl. Phys.*, 1958, **29**, 595–596.

32 N. Domingo, D. Fiorani, a M. Testa, C. Binns, S. Baker and J. Tejada, *J. Phys. D. Appl. Phys.*, 2008, **41**, 134009.

33 D. Peddis, C. Cannas, G. Piccaluga, E. Agostinelli and D. Fiorani, *Nanotechnology*, 2010, **21**, 125705 1–10.

34 M. Blancomantecon and K. Ogrady, *J. Magn. Magn. Mater.*, 2006, **296**, 124–133.

35 R. Mathieu, P. Svedlindh, R. Chakalov and Z. Ivanov, *Phys. Rev. B*, 2000, **62**, 3333–3339.

36 N. Zhang, W. Ding, W. Zhong, D. Xing and Y. Du, *Phys. Rev. B*, 1997, **56**, 8138–8142.

37 L. Balcells, J. Fontcuberta, B. Martínez and X. Obradors, *Phys. Rev. B*, 1998, **58**, R14697–R14700.

38 P. Dey and T. Nath, *Phys. Rev. B*, 2006, **73**, 214425.

39 D. Varshney and M. A. Dar, *J. Alloys Compd.*, 2015, **619**, 122–130.

Table 1

Table 1. The average coherent crystalline domain size <D_{XRD}> and the CFO / LCMO perceptual evaluated by a Rietveld refinement performed by MAUD software.

Sample	***<D_{XRD}> CFO***	***<D_{XRD}> LCMO***	***CFO (± 10 %)***	***LCMO (± 10 %)***
N-LCMO	-	28(1) nm	-	100 %
N-CFO	5(1) nm	-	100 %	-
N-MIX	10(1) nm	43(1) nm	30 %	70 %
NC	6(1) nm	32(1) nm	40 %	60 %

Uncertainties in the last digit are given in parenthesis.

Table 2

Table 2. The coercive ($\mu_0 H_C$) and the saturation field ($\mu_0 H_{sat}$), the susceptibility measured at 5 T ($dM/d\mu_0 H$), the average switching field ($\mu_0 H_C^{SFD}$) and the reversal field ($\mu_0 H_{rev}$) measured at 5 K.

Sample	***$\mu_0 H_C$ (T)***	***$\mu_0 H_{sat}$ (T)***	***$dM/d\,\mu_0 H$ ($A\ m^2\ kg^{-1}\ T^{-1}$)***	***$\mu_0 H_C^{SFD}$ (T)***	***$\mu_0 H_{rev}$ (T)***
N-LCMO	0.050(1)	0.3(1)	0.05(1)	0.05(1)	0.07(1)
N-CFO	0.83(1)	3.2(4)	1.55(7)	1.10(1)	0.85(5)
N-MIX	0.067(1)	3.4(6)	0.26(1)	0.05(2) 1.71(2)	0.07(1) 1.83(5)
NC	0.94(1)	3.1(1)	1.5(2)	0.42(5) 0.31(5)	1.25(5)

Uncertainties in the last digit are given in parenthesis.

.

TOC

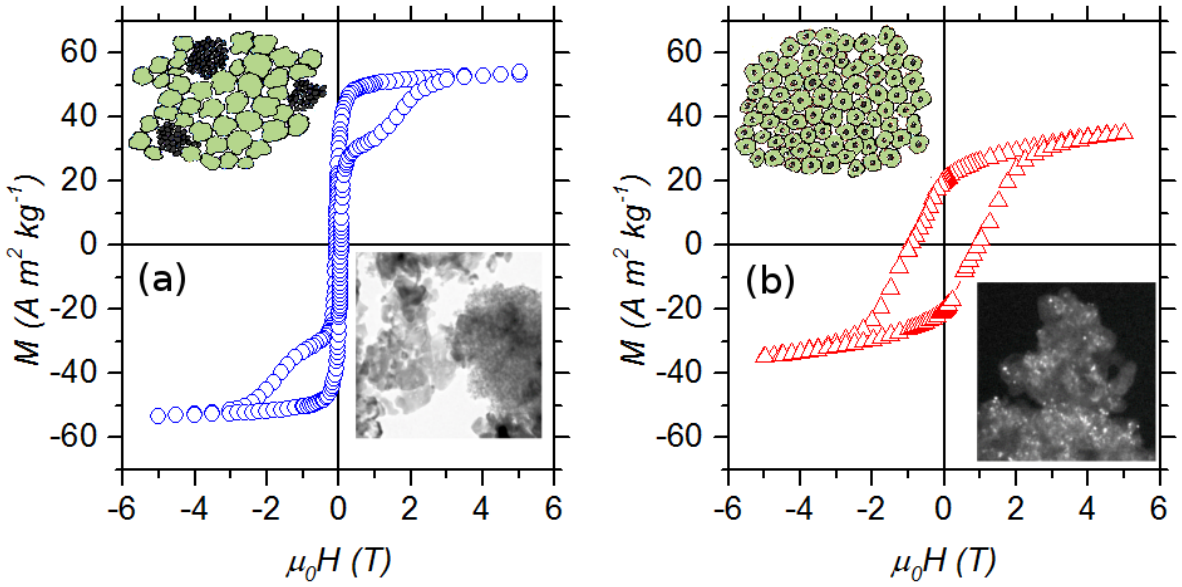

Two nanocomposites of $La_{0.67}Ca_{0.33}MnO_3$ and $CoFe_2O_4$ oxides have been prepared by mechanical mixing (a) and core/shell-like (b) approach, producing specific magnetic and magneto-electric behaviors.

Figure 1

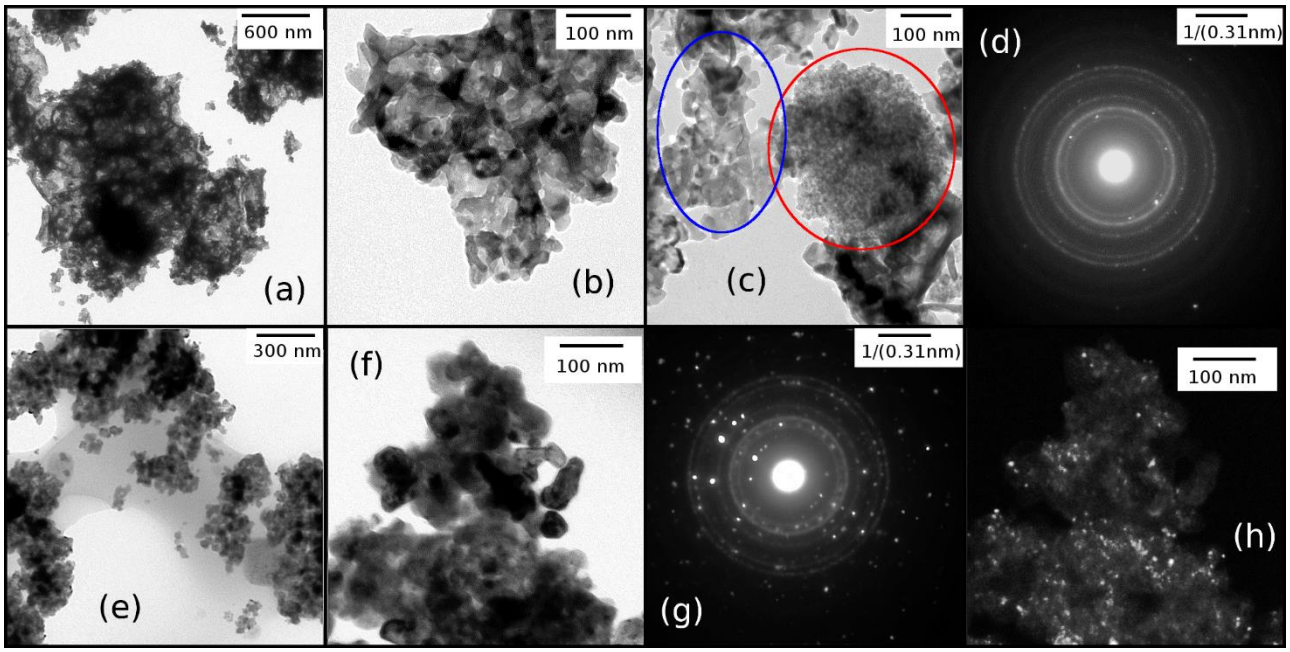

Figure 1: TEM images of sample N-MIX are shown in panel (a), (b) and (c), where the red and blue circles identify the CFO and LCMO particles aggregates, respectively. Panel (d) reports the ~~selected area electron diffraction~~ ~~(SAED)~~ pattern corresponding to the red-circled area. The structure of sample NC is shown in panels (e) and (f). The SAED pattern, corresponding to the sample area imaged in this last panel, is reported in panel (g); the CFO particles presence can be detected by dark-field images as in panel (h).

Figure 2

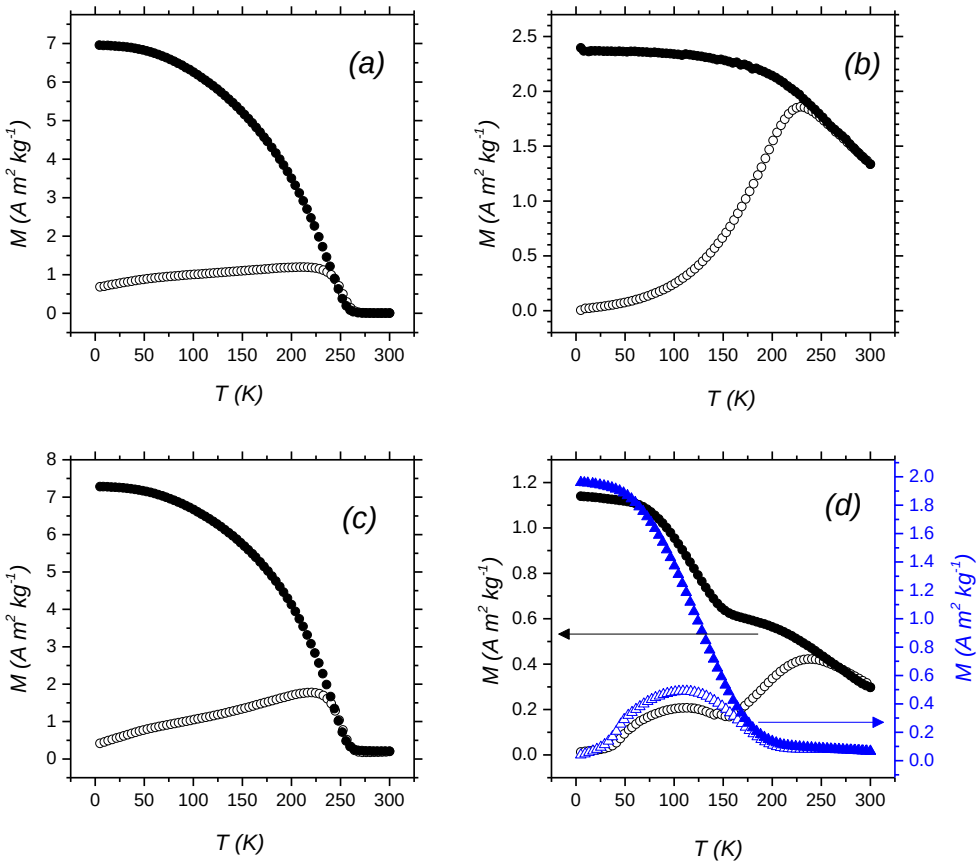

Figure 2. The ZFC and FC curves (empty and full symbols, respectively), for sample N-LCMO (a), N-CFO (b) and N-MIX are shown (c). Panel (d) reports the ZFC-FC curves of sample NC (empty and full black circles) and NC2 (empty and full black triangles). All curves were measured with an applied field of 2.5 mT.

Figure 3

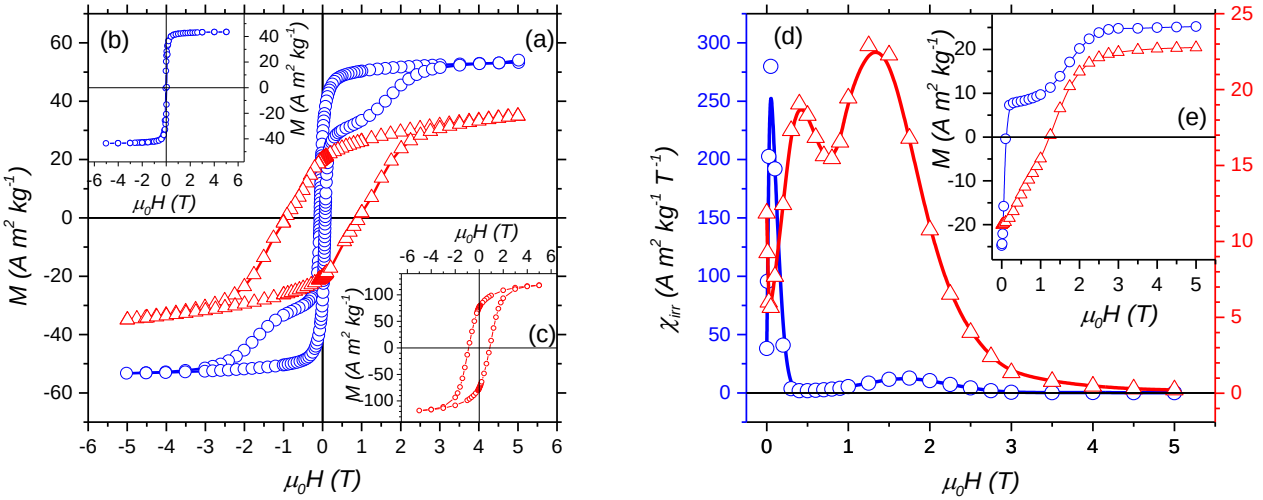

Figure 3. (a) M Vs H curves of N-MIX (blue circles) and NC (red triangles) samples. The N-LCMO (b) and N-CFO (c) single phases are reported for comparison. (d) Switching field distributions for sample N-MIX (blue circles) and NC (red triangles), as obtained from the first order derivative of the DCD curves, which are reported in the inset (e). All curves were measured at a temperature of 5 K.

Figure 4

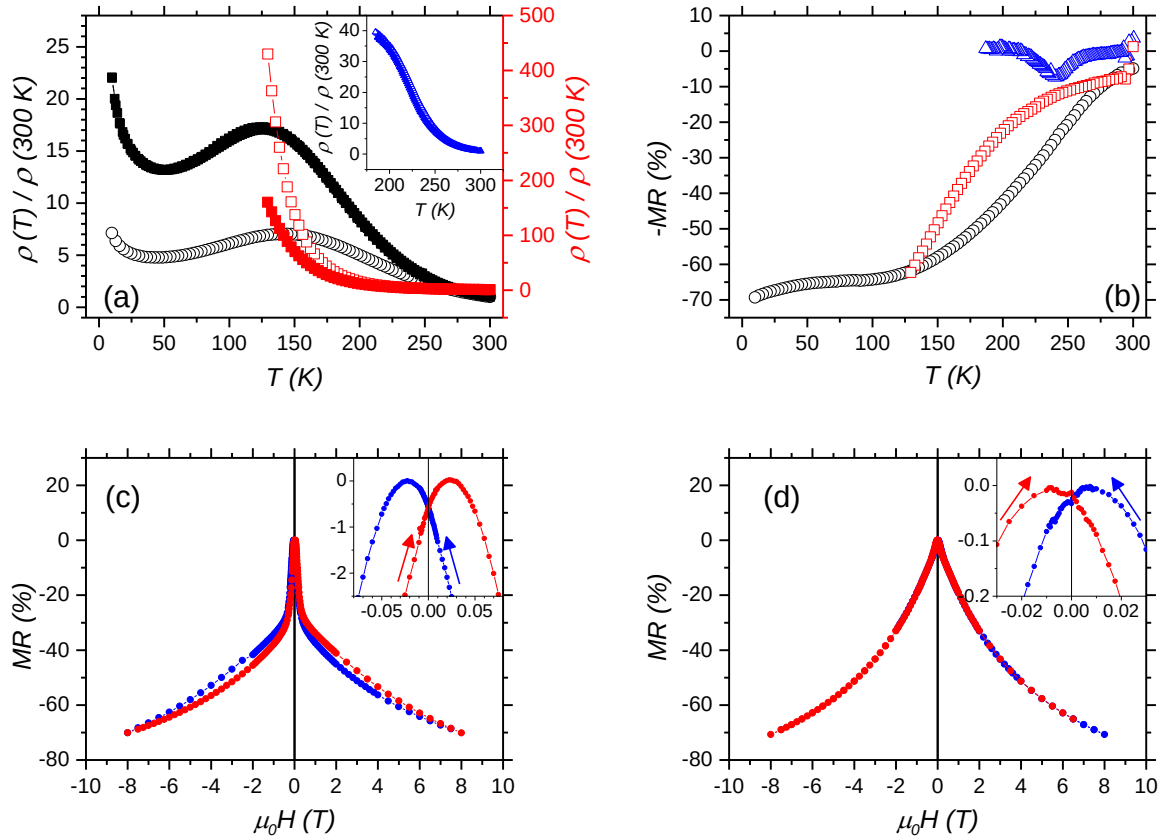

Figure 4. The temperature dependence of the resistance is reported for sample N-MIX (black circles), NC (blue triangles) and NC2 (red squares) in panel (a) without (empty symbols) and with a 5 T magnetic field applied (full symbols). It is important to note that for sample NC the two curves are almost perfectly superimposed. Panel (b) reports the temperature dependence of the magnetoresistance for N-MIX (black circles), NC (blue triangles) and NC2 (red squares). For sample N-MIX, the magneto-resistance measured at 5 and 150 K are reported in panel (c) and (d), respectively. A magnification at low field is reported in the respective insets, with arrows indicating the direction of field sweeping.